2

Relaxor-ferroelectric PMN–PT Thick Films

Hana Uršič and Marija Kosec
Electronic Ceramics Department, Jožef Stefan Institute
Slovenia

1. Introduction

Electroceramic thick films are 2D (planar) structures that, in their simplest form, consist of a substrate, a bottom electrode, a ceramic film and a top electrode, with the thickness of an individual layer being typically between 1 and 100 μm. The processing of thick films is similar to the processing of bulk ceramics, i.e., it involves powder synthesis, shaping and sintering. The major difference, however, is in the clamping of the film onto the substrate. The consequences of this are a constrained sintering, a possible reaction with the electrode or the substrate during firing, and the thermal stresses that are generated during the cooling. To minimize the chemical interaction of the film and the substrate the sintering temperature must be kept relatively low in comparison to that for the bulk. This requires a fine particle size for the powder and additives that form a liquid phase at the sintering temperature. This liquid phase must also be present to enable the densification under the constrained conditions, as was predicted and demonstrated in Kosec et al. (1999).

The effect of clamping the active film to the relatively stiff substrate results in smaller displacements in comparison to substrate-free structures. Due to the mismatch of the thermal expansion of the thick-film and substrate materials during the processing the properties of the thick films differ from those of the respective bulk ceramics. Furthermore, an additional drawback can be the deterioration of the thick film's properties due to its chemical interaction with the substrate. To ensure a sufficient displacement required for a certain application, different solutions have been proposed, such as a reduction in the thickness of the substrate, the processing of thick-film multilayer structures or the preparation of "substrate-free" structures.

In the world of technology there is a continuous, global increase of interest in the miniaturisation of devices, materials and system integration. Thick-film structures are a good example of the opportunities offered for the miniaturization of electromechanical systems by the successful implementation of new functional materials and technologies. Driven by the versatility of conventional thick-film technology, the processing of functional structures with thick films on different substrates is possible, along with many design possibilities.

In this chapter the progress in relaxor-ferroelectric $Pb(Mg_{1/3}Nb_{2/3})O_3$–$PbTiO_3$ (PMN–PT) thick films is reported. The preparation procedures, the processing of PMN–PT thick films on different substrates, the structural and electrical characterization as well as PMN–PT thick-film devices are discussed. The phase composition and functional properties of PMN–PT thick films are discussed in terms of the thermal stresses generated in the films during

the thermal treatment. Due to these process-induced stresses the electrical and structural properties of the films can be changed dramatically in comparison to the unstressed films. Some representative examples of PMN–PT thick-film applications are described, including a novel approach to the manufacture of large-displacement "substrate-free" PMN–PT/Pt actuators using thick-film technology.

2. Relaxor-ferroelectric PMN–PT material

Ferroelectric and piezoelectric films are mostly based on lead oxide compounds, mainly $Pb(Zr,Ti)O_3$ (PZT) solid solutions. An alternative to PZT are the relaxor-based systems, where the term relaxor-ferroelectrics is used for solid solutions between relaxors such as $Pb(Mg_{1/3}Nb_{2/3})O_3$ (PMN) and ferroelectrics such as $PbTiO_3$ (PT) (Cross, 1987; Damjanovic, 2008). One of the most widely studied relaxor-ferroelectrics is $Pb(Mg_{1/3}Nb_{2/3})O_3$–$PbTiO_3$ (PMN–PT). These PMN–PT-based materials are characterized by a high dielectric permittivity, high piezoelectric properties, a high electrostriction, and are suitable for applications in multilayer capacitors, actuators, sensors and electro-optical devices (Park & Shrout, 1997a, 1997b).

The morphotropic phase boundary (MPB) in the $(1\text{-}x)Pb(Mg_{1/3}Nb_{2/3})O_3$–$xPbTiO_3$ system is located close to the x=0.35 composition. The strong piezoelectric properties are related to the "polarization rotation" between the adjacent rhombohedral phase with the space group R3m (subsequently referred to as the rhombohedral R3m phase in the text) and tetragonal phase with the space group P4mm (subsequently referred to as the tetragonal P4mm phase) through one (or more) intermediate phase(s) of low symmetry, i.e., a monoclinic (orthorhombic or triclinic) phase (Davis et al., 2006; Noheda et al., 2001). As a consequence, the observation of a low-symmetry phase, e. g., a monoclinic phase, may suggest strong electromechanical responses.

It was shown (Singh & Pandey, 2003) that the MPB region of the PMN–PT ceramic material contains two monoclinic phases with the space groups Cm (subsequently referred to as the monoclinic Cm phase) and Pm (subsequently referred to as the monoclinic Pm phase) stable in the composition ranges $0.27 < x < 0.30$ and $0.31 < x < 0.34$, respectively. For ceramics of the composition $x = 0.35$, the coexistence of the monoclinic Pm and the tetragonal P4mm phases was reported (Alguero et al., 2006, 2007; Carreaud et al., 2005; Singh & Pandey, 2003; Uršič et al., 2011a), stressing that the phase composition ratio between the monoclinic and the tetragonal phases depends on different parameters, such as the grain-size effect (Alguero et al., 2006, 2007; Carreaud et al., 2005) and the poling field (Uršič et al., 2011a) of the ceramics.

PMN–PT ceramics and a single crystal with its composition on the MPB can have the piezoelectric coefficients d_{33} as high as 700 pC/N (Kelly et al., 1997; Xia et al. 2007) and 1500–2800 pC/N (Park & Shrout, 1997a; Shrout et al., 1990; Zhang et al., 2001), respectively. The commonly used poling electric fields for the PMN–PT material vary from 2 to 3.5 kV/mm (Alguero et al., 2006, 2007; Leite et al. 2002; Kelly et al., 1997; Xia et al. 2007). On the other hand, the PMN–PT material with compositions x=0–0.1 shows relaxor behaviour (Cross et al., 1987; Swartz et al., 1982; Swartz et al., 1984) and are known as good electrostrictive materials (Kighelman et al., 2001; Uchino et al., 1890; Vikhnin et al., 2003; Zhao et al., 1995). Likewise, the electrostrictive effect of the MPB compositions was also reported to be relatively high (Bokov & Ye, 2002). Furthermore, due to its large responses to an applied electric field, the PMN–PT material was investigated as a promising material for actuator applications (Uršič et al., 2011).

3. PMN–PT thick films

3.1 Processing of the PMN–PT thick films

The processing of relaxor or ferroelectric thick films has been discussed in the open literature by many authors. However, because of the lack of an assortment of commercially available thick-film materials and no conventional processing procedures the investigations made so far were carried out using different technological procedures and involved thick films with various compositions. The PMN–PT composition has recently been considered as an appropriate material for thick-film technology as it exhibits very good functional properties. The most commonly used method for the deposition of PMN–PT-based thick films is screen-printing (Akiyama et al., 1999; Gentil et al., 2004, 2005; Kosec et al., 2007, 2010; Uršič et al., 2008a, 2008b, 2010, 2011b). To form good-quality and high-performance PMN–PT thick films, a fine particle size of the PMN–PT powder is required. One way to prepare such powder is by mechanochemical synthesis (Kosec et al., 2007, 2010). In fig. 1 a (FE-SEM) micrograph and an X-ray diffraction (XRD) pattern of the 0.65PMN–0.35PT powder prepared by mechanochemical syntheses are shown. The families of planes for the 0.65PMN–0.35PT perovskite phase are given in brackets. It was shown by Rietveld refinement that the powder is not cubic; in fact the best fit was obtained for the monoclinic Pm phase. The particle size is sub-micrometre, i.e., the distribution is narrow with a median particle size d_{50} equal to 0.32 μm (Kosec et al., 2010).

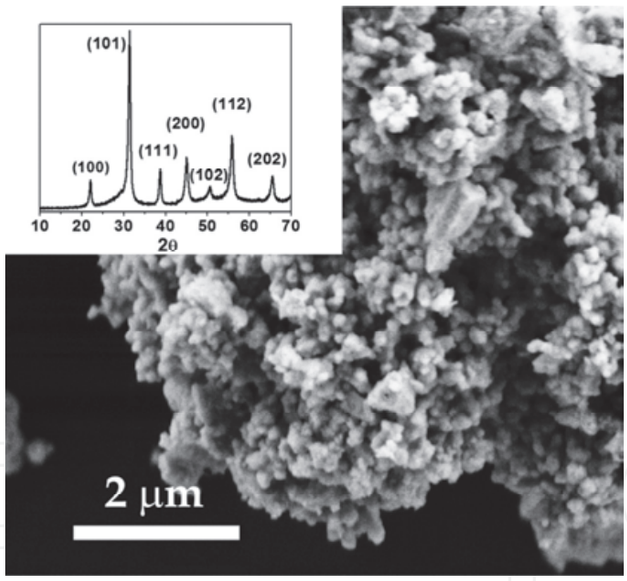

Fig. 1. The FE-SEM micrographs of 0.65PMN–0.35PT powder with 2 mol% excess of PbO prepared by mechanochemical synthesis. Inset: The XRD pattern of this powder. The families of the planes for the 0.65PMN–0.35PT perovskite phase are given in brackets.

For the screen-printing process the ceramic pastes are made by mixing the PMN–PT powder with different binders and organic carriers to obtain the suitable printability. The paste is then forced through the open areas of the screen onto the surface of the substrate. The scheme of the screen-printing procedure is shown in fig. 2 (top). After screen-printing the films are usually sintered for 2 h at temperatures between 800 and 1100°C (Gentil et al., 2004, 2005; Kosec et al., 2007, 2010; Uršič et al., 2008a, 2008b, 2010, 2011b). To minimize the

chemical interaction of the film and the substrate the sintering temperature is kept relatively low in comparison to that for the bulk ceramics, i.e., 1200°C. This requires additives that form a liquid phase at the sintering temperature.

To obtain a PMN–PT thick film with the desired functional response, the material has to be dense and without any secondary phase. In the literature the effect of different sintering aids on the densification of thick films was investigated and the best densification and a large increase in the grain size was obtained for the sintering aid $LiCO_3$ (Gentile et al., 2005). The other way that the densification of the PMN–PT can be aided is by the presence of the PbO-rich liquid phase originating from the starting composition containing an excess of PbO. To keep the liquid phase in the film a lead-oxide-rich atmosphere can be created, e. g., using a packing powder rich in PbO. In the literature the atmosphere was achieved with $PbZrO_3$ packing powder with an excess of PbO, short PZ/P (Gentil et al., 2004; Kuščer et al., 2008; Kosec et al., 2010; Uršič et al., 2088b, 2010) or with the packing powder PZ/P+PMN (Gentil et al., 2004). During heating the PbO sublimates from the high-surface-area packing powder, giving a PbO-saturated atmosphere around the thick film that keeps the PbO liquid in the film. Since the system is semi-closed, the PbO is lost slowly from the system, first from the powder and later from the film. Therefore, the time for which the liquid phase is present in the PMN–PT film depends on the amount of packing powder. The process is shown schematically in fig. 2 (bottom). The density of the films is proportional to the duration of the liquid-phase sintering and increases with the amount of packing powder, up to the limit where the amount of packing powder is too high, and after sintering of the film there is still enough PbO vapour to keep the PbO in the PMN–PT thick films (Kuščer et al., 2008; Kosec et al., 2010).

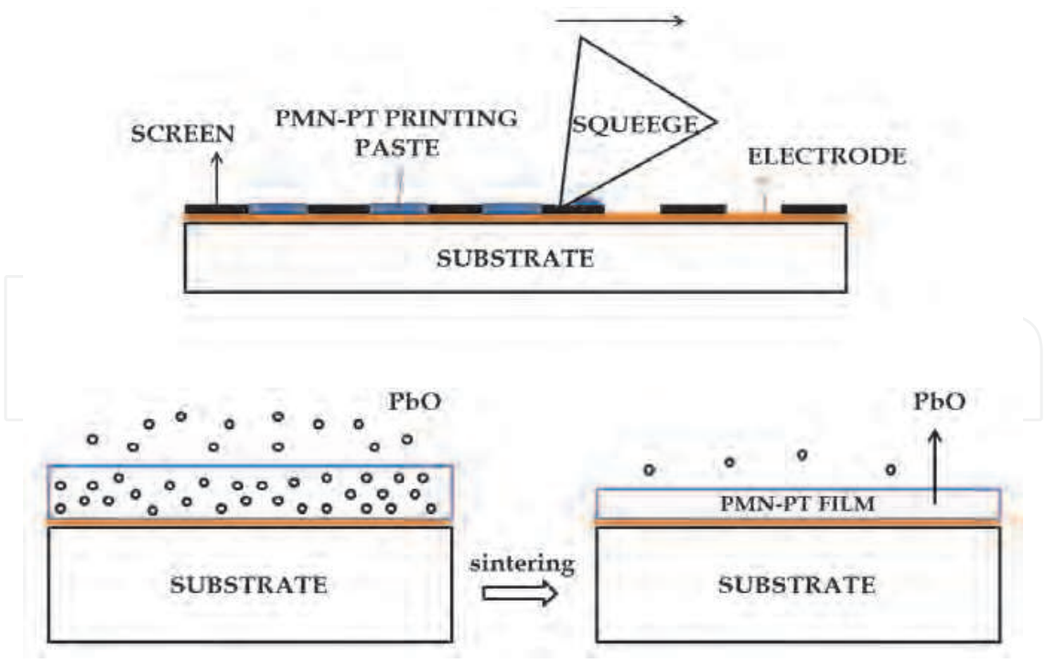

Fig. 2. The scheme of screen-printing (top) and sintering (bottom) of PMN–PT thick films.

In addition to the screen-printing, the successful experiments with electrophoretic deposition (Chen et al., 2009a, 2009b; Fan et al., 2009; Kuščer & Kosec, 2009), the hydrothermal process

(Chen et al., 2008) and sol-gel (Wu et al., 2007; Zhu et al., 2010) were reported. The PMN–PT thick-films were also prepared as single crystals by a modified Bridgman method and after the preparation they were bonded on Si substrates (Peng et al., 2010).
The proper selection of the materials, including the compatibility of the functional material with the electrodes and the substrates, is among the most important for the successful processing of thick-film structures. The most common substrate material used for PMN–PT thick films is polycrystalline Al_2O_3 (alumina) (Gentil et al., 2004, 2005; Kosec et al., 2007, 2010; Uršič et al., 2008a, 2008b, 2010, 2011b, Fan et al., 2009; Kuščer & Kosec, 2009). However, PMN–PT- and PMN-based thick films were also processed on Si (Gentil et al., 2004; Wu et al., 2007; Zhu et al., 2010), Pt Pt (Chen et al., 2009a, 2009b; Uršič et al., 2008, 2010), Ti (Chen et al., 2008), AlN (Uršič et al., 2010) and PMN–PT (Uršič et al., 2010, 2011b) substrates. In fig. 3 the photographs and the scanning-electron-microscope (SEM) micrographs of the 0.65PMN–0.35PT thick-film on the alumina substrate are shown. In order to prevent the chemical interactions between the PMN–PT film and the alumina substrate a $PbZr_{0.53}Ti_{0.47}O_3$ (PZT) barrier layer was processed between the substrate and the bottom electrode (fig. 3(c)) (Kosec et al., 2010; Uršič et al., 2010). The use of a PZT-based barrier layer to prevent any film/substrate interactions has been proposed before for (Pb,La)(Ti,Zr)O_3 (PLZT) thick films on alumina substrates (Holc et al., 1999; Kosec et al., 1999).

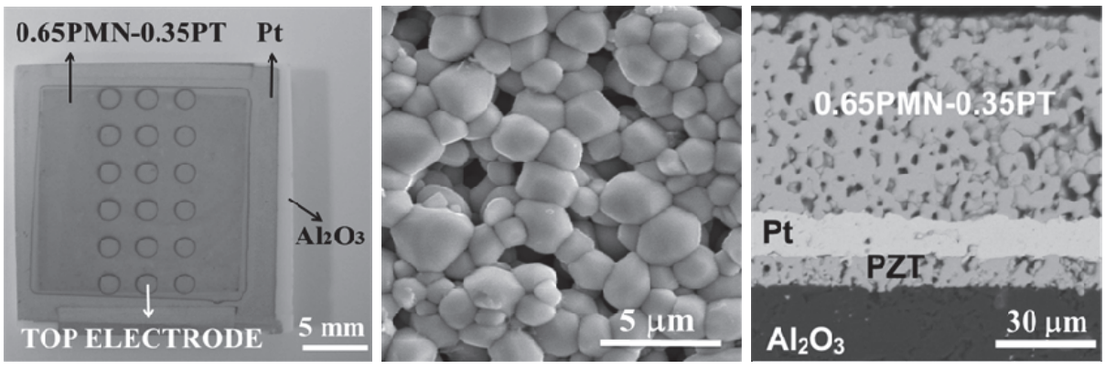

(a) (b) (c)

Fig. 3. (a) Photograph of the 0.65PMN–0.35PT thick film on Al_2O_3 substrate. SEM micrographs of (b) the surface and (c) the cross-section of the 0.65PMN–0.35PT thick film on Al_2O_3 substrate. The bottom electrode is Pt and the top electrode is sputtered Au. The PZT barrier layer is interposed between the Al_2O_3 substrate and the Pt electrode.

3.2 Structural and electrical properties of PMN–PT thick films clamped on rigid substrates

In comparison with PMN (Gentil et al., 2004) and 0.80PMN–0.20PT (Chen et al., 2009b) thick films that exhibit relaxor behaviour, the 0.65PMN–0.35PT thick films on alumina substrate show ferroelectric behaviour (Gentil et al., 2004; Kosec et al., 2007; Uršič et al., 2008b). However, the properties of PMN–PT thick films depend not only on the material composition, but also on the compatibility of the functional materials with the electrodes, adhesion layers, substrate materials and technological parameters relating to their processing (Gentil et al., 2005; Uršič et al., 2010, 2011b). The films processed on substrates at elevated temperatures and cooled to room temperature are thermally stressed, due to the mismatch between the thermal expansion coefficient (TEC) of the film and the substrate.

Recent investigations (Uršič et al., 2010, 2011b) showed that due to the process-induced thermal stresses the structural and electrical properties of PMN–PT thick films with the MPB composition can be changed dramatically in comparison to the unstressed films.

For sake of clarity we now focus on 0.65PMN–0.35PT thick films on thick Al_2O_3 and 0.65PMN–0.35PT substrates prepared under identical processing conditions, i.e., sintered at 950°C for 2 h and then cooled to room temperature. After cooling to room temperature the films on the Al_2O_3 substrates are under compressive thermal stress, while the TEC of the substrate is higher than the TEC of the film. The basic equation for the thermal stress in a film clamped to a substrate, regardless of the film's thickness, is (Ohring, 1992):

$$\sigma_f(T) = (\alpha_s - \alpha_f)(T_2 - T_1)Y_f/(1 - \nu_f), \quad (1)$$

where α_s is the TEC of the substrate (K^{-1}), α_f is the TEC of the film (K^{-1}), Y_f is the Young`s modulus of the film ($N/m^2$) and $\nu_f$ is the Poisson`s ratio of the film. If the films are cooled down to room temperature then T_1 is the processing temperature (K), T_2 is room temperature (K) and $\Delta T = T_2 - T_1$ is the temperature difference (K). Normally, thick films are considered in the same way as thin films; however, in the case of thick films, the thickness of the film plays an important role, and this fact cannot be neglected, as we have been able to demonstrate in Uršič et al., (2011b). The compressive residual stress in the 0.65PMN–0.35PT films on Al_2O_3 substrates calculated from the basic eq. (1), regardless of the film thickness, is -168.5 MPa.

To evaluate the compressive thermal stress with respect to the film thickness, the *x* component of the thermal stress σ (the component parallel to the film surface σ_x) of a 0.65PMN–0.35PT thick film on an Al_2O_3 substrate was calculated using the finite-element (FE) method. The FE analysis of the stress was performed in two steps. First, the influence of the bottom Pt electrode and the PZT barrier layer were neglected. Fig. 4 (a) shows the distribution of the σ_x obtained for the 20-µm-thick 0.65PMN–0.35PT film on a rigid 3-mm-thick Al_2O_3 substrate. Due to the symmetry, the *y* component of the stress (σ_y) is equal to the *x* component σ_x. In fig. 4 (b) the σ_x vs. the position on the top surface of the 20-µm- and 100-µm-thick films is shown. The red line in fig. 4 (a) shows the coordinates (x, $y = 0$, $z = 20$ or 100) where the σ_x presented in fig. 4 (b) was calculated. The calculated stress σ_x in the film is compressive, with a value in the central position on the top surface ($x = 0$, $y = 0$, $z = 20$ or 100) of -167.4 MPa and -162.7 MPa for the 20-µm- and 100-µm-thick films, respectively. The decrease of the σ_x on the boundaries of the films, see fig. 4 (b), is due to the free boundary condition.

In the second step the influences of the PZT barrier and the Pt bottom-electrode layers were studied. For this reason, the FE model was updated accordingly. The σ_x on the top surface of the 20-µm- and 100-µm-thick films for both models (with and without the Pt and PZT layers) is shown in fig. 4 (c). No major difference was observed between the solutions of these two models, which means that the thin PZT barrier layer and the Pt bottom electrode do not have much influence on the stress conditions in the 0.65PMN–0.35PT film on the rigid 3-mm-thick Al_2O_3 substrate. The calculated values for σ_x in the central position on the top surface of the film ($x = 0$, $y = 0$, $z = 20$ or 100) for the updated model are -168.1 MPa and -163.3 MPa for the 20-µm- and 100-µm-thick films, respectively (Uršič et al., 2011b).

In contrast, in the case of 0.65PMN–0.35PT films on 0.65PMN–0.35PT substrates, the film and substrate are made from the same material and therefore there is no mismatch between the TEC of the film and the substrate, hence the films on 0.65PMN–0.35PT substrates are not stressed. Fig. 5 shows SEM micrographs of the 0.65PMN–0.35PT thick-film surface and the cross-section of the film on the 0.65PMN–0.35PT substrate.

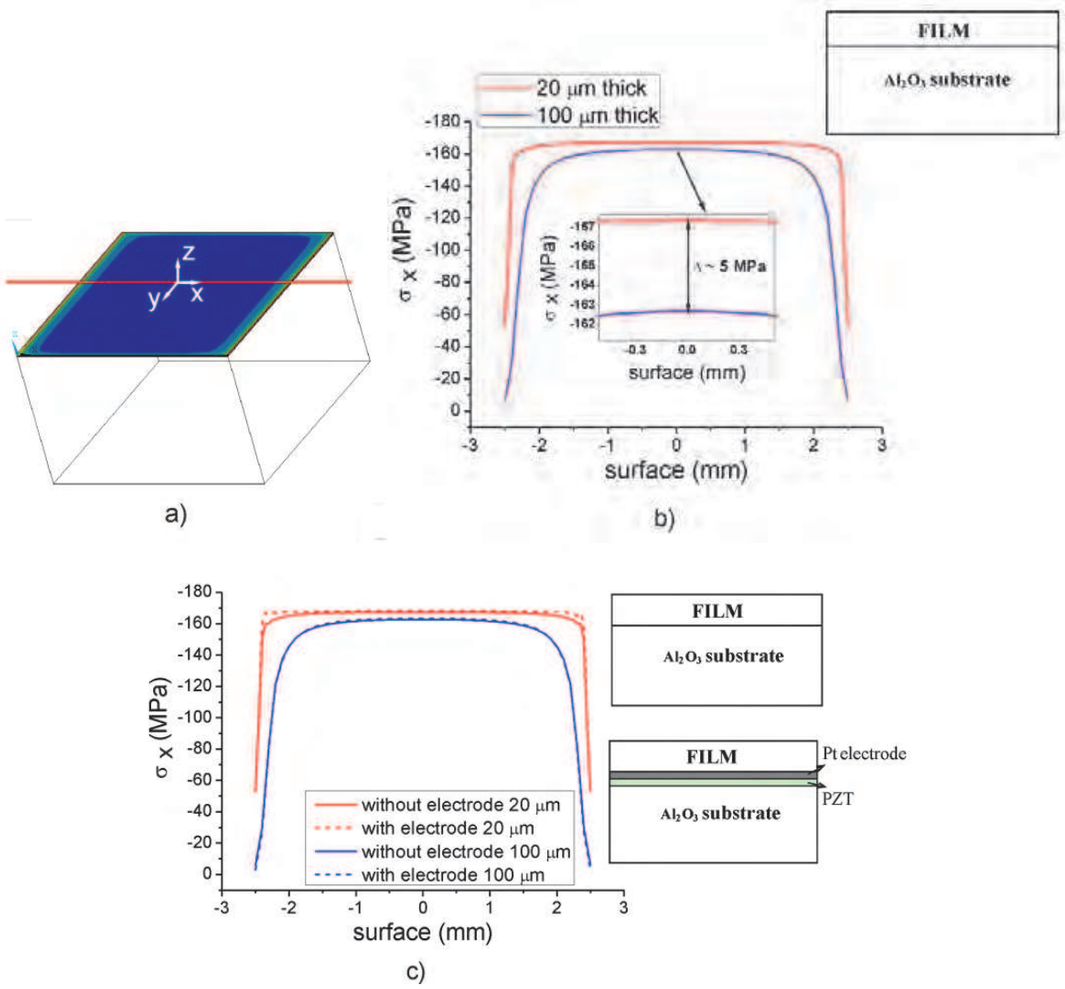

Fig. 4. (a) The model structure of the 0.65PMN–0.35PT film clamped on the thick alumina substrate and the σ_x distribution. The line shows the coordinates (x, y = 0, z = top surface), where σ_x was calculated. (b) The σ_x vs. the position on the top surface of the 20-μm- and 100-μm-thick films. Inset: The enlarged central part of the graph. (c) The comparison of the σ_x shown in (b) with the updated calculation made for the structure including the Pt bottom electrode and the PZT barrier layer. Right: Schemes of the cross-section of the film-substrate structure (Reprinted with permission from [Uršič., H. et al., J. Appl. Phys. Vol. 109, No. 1.]. Copyright [2011], American Institute of Physics).

The 0.65PMN–0.35PT films on Al_2O_3 substrates were sintered to a high density with a coarse microstructure, as can be seen in figs. 3 (b) and (c). The median grain size of these films is 1.7 μm ± 0.6 μm. In contrast, the films on the 0.65PMN–0.35PT substrates were sintered to a lower density and the microstructure consists of smaller grains, i.e., 0.5 μm ± 0.2 μm (figs. 5 (a) and (b)). Hence, the substrates on which the films are clamped influence the microstructure of the films (Uršič et al., 2010).

Furthermore, in PMN–PT material the MPB shifts under the compressive stress (Uršič et al., 2011b). In figs. 6 (a) and (b) the measured XRD spectrum, the XRD spectrum calculated by a Rietveld refinement and the measured XRD spectra in the range from 2θ = 44.4° to 2θ = 45.7° are shown for 0.65PMN–0.35PT films on Al_2O_3 and 0.65PMN–0.35PT substrates.

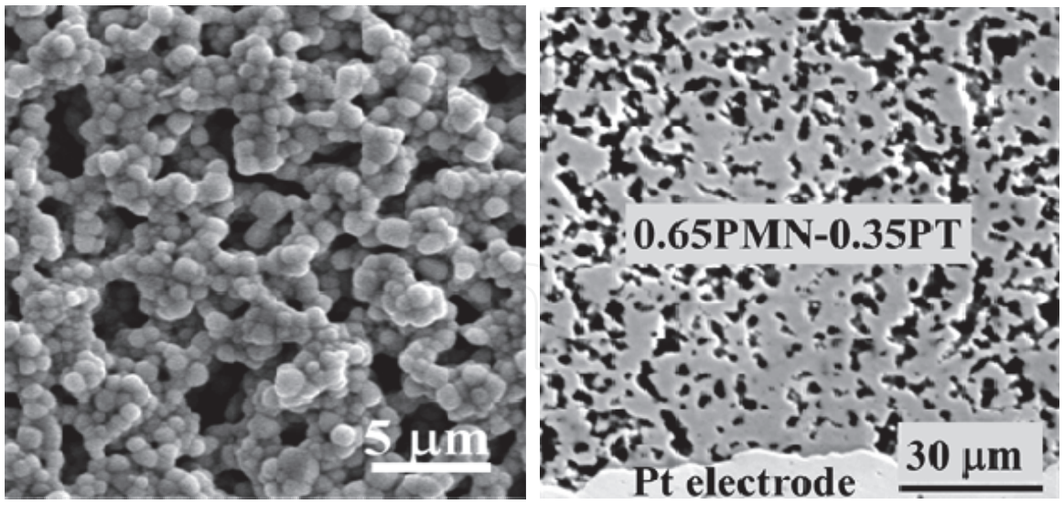

(a) (b)

Fig. 5. SEM micrographs of (a) the surface and (b) the cross-section of the 0.65PMN–0.35PT thick film on the 0.65PMN–0.35PT substrate. The bottom electrode is Pt and the top electrode is sputtered Au.

The phase composition of the 0.65PMN–0.35PT films under compressive stress is a mixture of the monoclinic Pm and tetragonal P4mm phases, while the non-stressed films are monoclinic Pm (Uršič et al., 2010, 2011b). This is in agreement with previous results reported for bulk 0.65PMN–0.35PT ceramics, where it is shown that the ceramics with larger gains consist of the monoclinic Pm and tetragonal P4mm phases, while the ceramics with submicron grains are mainly monoclinic Pm (Alguero et al., 2007). In addition to the grain size effect, in thick films the residual compressive stresses also influence the phase composition of the films. This can be clearly seen from the fact that the higher percentage of tetragonal P4mm phase is obtained for films on Al_2O_3 substrates rather than for "stress-free" bulk ceramics sintered at 1200°C with a similar grain size. The 20-μm-thick film on the Al_2O_3 substrate that is under a stress of -168.1 MPa contains 58% of the tetragonal phase and the rest is monoclinic phase, while the "stress-free" bulk ceramic with the same composition and similar grain size contains only 14% of the tetragonal phase. Furthermore, if the 0.65PMN–0.35PT film on the Al_2O_3 substrate is thicker (for example, 100 μm), it contains more monoclinic phase, which is more like the phase composition of the "stress-free" bulk ceramic (Uršič et al., 2011b).

The dielectric constant (ε) vs. temperature and the hysteresis loops of 0.65PMN–0.35PT thick films under compressive stress (films on Al_2O_3 substrates) and unstressed films (films on 0.65PMN–0.35PT substrates) are shown in fig. 7. The films under compressive stress show ferroelectric behaviour; the phase-transition peak between the high-temperature (HT) cubic phase and the tetragonal P4mm phase is sharp, with the maximum value of the dielectric constant ε_{max} = 20,500 at 1 kHz and no dependence of the peak temperature (T_{max}) at which ε_{max} is achieved can be observed (Uršič et al., 2008b). These films show saturated ferroelectric hysteresis loops with a remnant polarization P_r of 21 μC/cm². While the HT phase-transition peak of the unstressed films is broader, the ε_{max} is only 2100 at 1 kHz. For these films the P_r is 8 μC/cm².

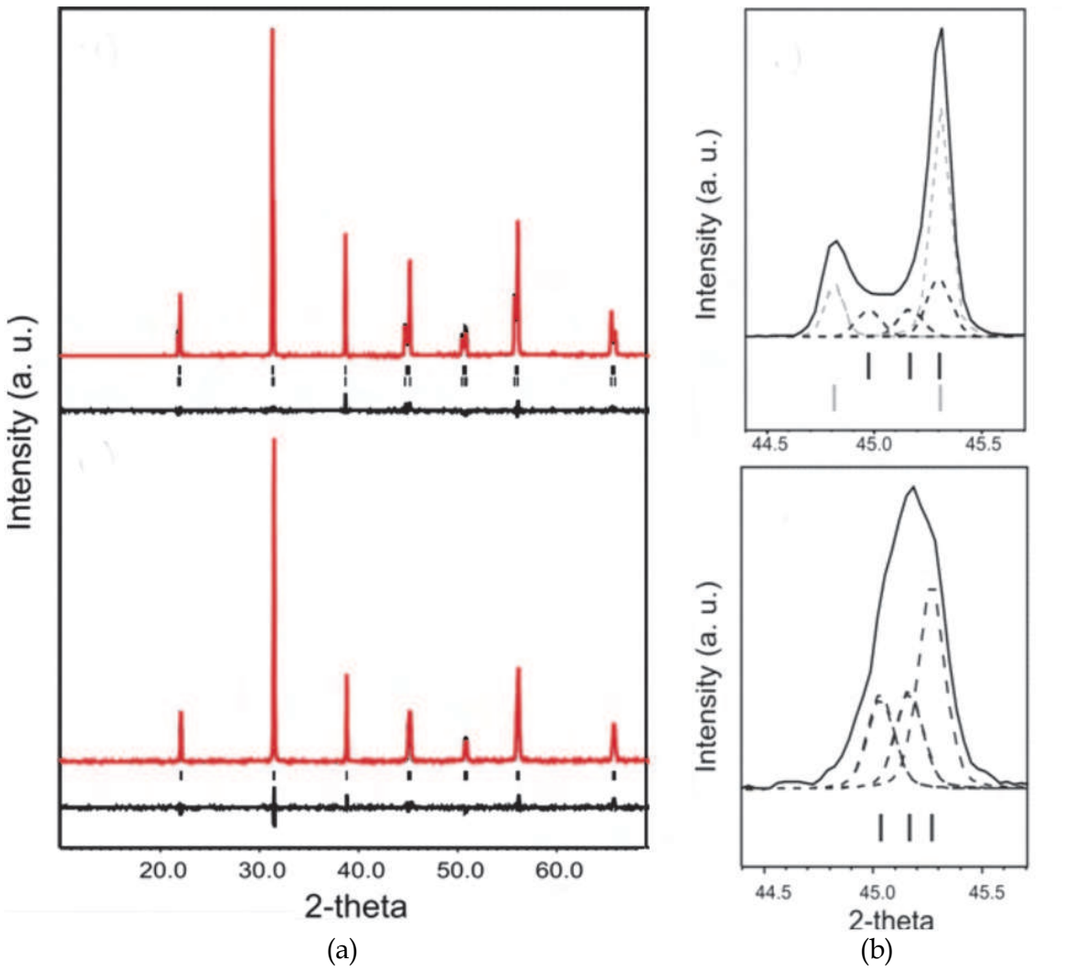

Fig. 6. (a) Measured (red), calculated (black) and difference (black curve at the bottom) curves of the XRD Rietveld refinement for 0.65PMN–0.35PT films deposited on Al_2O_3 (top) and 0.65PMN–0.35PT (bottom) substrates. The top marks correspond to the tetragonal phase and the bottom ones to the monoclinic. (b) XRD diagrams of 0.65PMN–0.35PT thick films on Al_2O_3 (top) and 0.65PMN–0.35PT (bottom) substrates in the range from $2\theta = 44.4°$ to $2\theta = 45.7°$. The refined peak positions of the (002), (200) tetragonal (grey) and the (002), (200), (020) monoclinic (black) phases are marked. (Reprinted from J. Eur. Ceram. Soc., 30/10, Uršič, H. et al., Influence of the substrate on the phase composition and electrical properties of 0.65PMN–0.35PT thick films, pp. (2081–2092), Copyright (2010), with permission from Elsevier)

Similar behaviour was reported for the 0.65PMN–0.35PT bulk ceramic. The 0.65PMN–0.35PT ceramics show ferroelectric behaviour. However, when the average grain size of the 0.65PMN–0.35PT ceramics decreases to the submicron range and approaches the nanoscale, relaxor-type behaviour is observed down to room temperature, which causes a strong decrease in the electrical polarization (Alguero et al., 2007). From fig. 7 it can be clearly seen that the grain size effect also influences the properties of 0.65PMN–0.35PT thick films, in a similar way as in bulk ceramics, while the median grain size of films on the Al_2O_3 and 0.65PMN–0.35PT substrates is 1.7 μm and 0.5 μm, respectively. However, the reason for

lower properties of the films on the 0.65PMN–0.35PT substrates is also the lower density of these films.

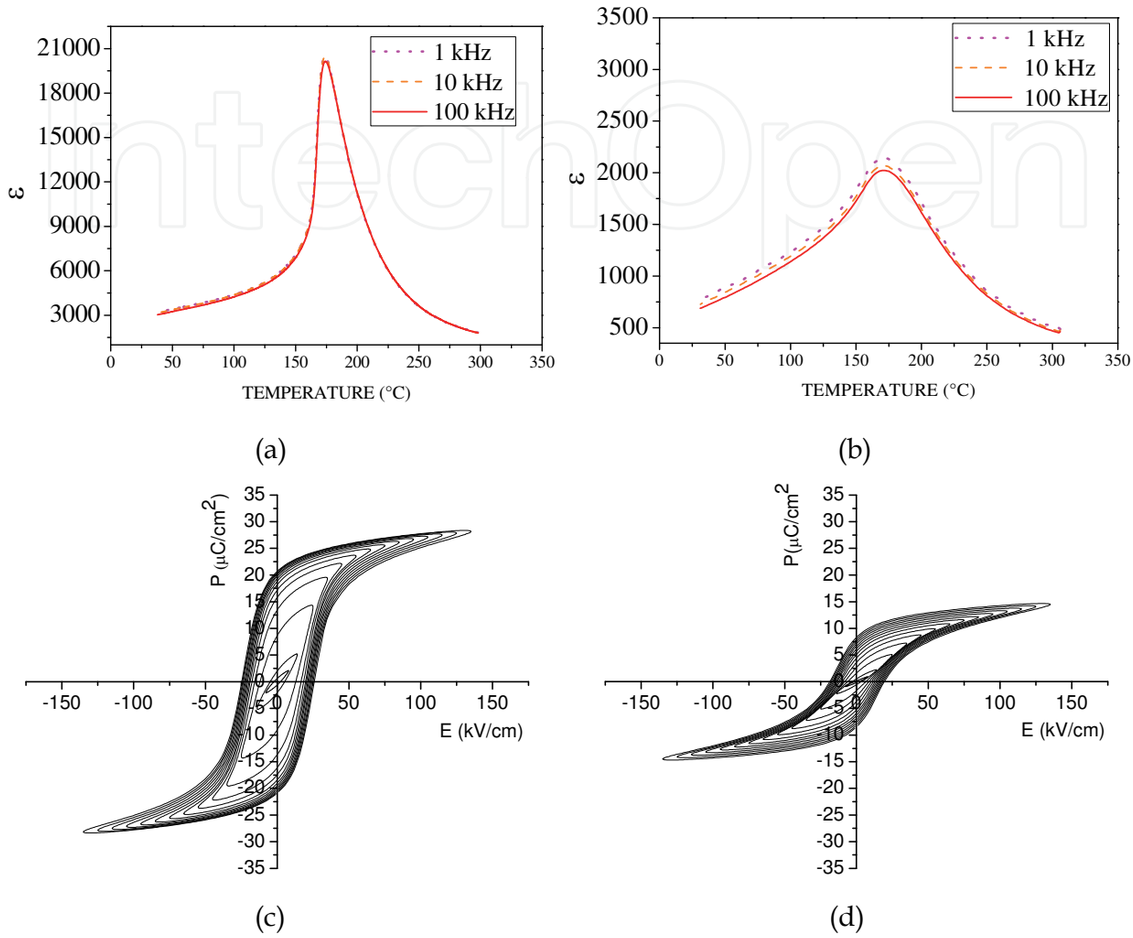

Fig. 7. The dielectric constant (ε) vs. temperature for 0.65PMN–0.35PT (a) thick films under compressive stress and (b) unstressed films. The hysteresis loops for 0.65PMN–0.35PT (c) thick films under compressive stress and (d) unstressed films.

3.3 Piezoelectric and electrostrictive properties of PMN–PT thick films

As already mentioned, the PMN (Gentil et al., 2004) and 0.80PMN–0.20PT (Chen et al., 2009b) thick films exhibit relaxor behaviour. These compositions are known to be good electrostrictive materials, while the 0.65PMN–0.35PT thick films on alumina substrates show ferroelectric and piezoelectric behaviour (Gentil et al., 2004; Kosec et al., 2007).

In piezoelectric and ferroelectric materials the mechanical stress T and the strain S are related to the dielectric displacement D and the electric field E, as indicated in the constitutive equations:

$$\{S\} = \left[s^{E}\right]\{T\} + [d]\{E\} \tag{2}$$

$$\{D\} = [\mathrm{d}]^{\mathrm{T}} \{T\} + \left[\varepsilon^{T}\right] \{E\} \tag{3}$$

where $[s^E]$ is the compliance matrix evaluated at a constant electric field, $[\varepsilon^T]$ is the permittivity matrix evaluated at a constant stress and [d] is the matrix of the piezoelectric coefficients.

The successful design of thick-film structures for various applications can take place only with a thorough knowledge of the electrical and electromechanical properties of the thick film. Since the effective material properties of the thick film depend not only on the material composition but also on the compatibility of the thick-film material with the substrate, the characterisation of the piezoelectric thick films is required before the design phase. Because of a lack of standard procedures for the characterization of thick films, special attention has to be paid to providing the actual material parameters. In order to obtain proper material parameters some unconventional characterisation approaches have been used, such as a nano-indentation test for the evaluation of the compliance parameters (Uršič et al., 2008a; Zarnik et al., 2008) or some standard-less methods for a determination of the piezoelectric coefficients of the thick films (Uršič et al., 2008a, 2008c).

The piezoelectric coefficients of the thick films differ from the coefficients of the bulk ceramics with the same composition. One of the main reasons for this is that the films are clamped by the substrates. For a clamped film the ratio D_3/T_3 does not represent the piezoelectric coefficient d_{33} of the free sample, but an effective piezoelectric coefficient d_{33}^{eff} (Lefki & Dormans; 1994):

$$\mathrm{d}_{33}^{eff} = \mathrm{d}_{33} - 2\mathrm{d}_{31} \frac{\frac{\mathrm{v_s}}{\mathrm{Y_s}} + \mathrm{s}_{13}^{E}}{(\mathrm{s}_{11}^{E} + \mathrm{s}_{12}^{E})}, \tag{4}$$

where d_{33} and d_{31} are the direct and the transverse piezoelectric coefficients, respectively, (C/N), s^E_{13}, s^E_{11}, s^E_{12} are the elastic compliance coefficients at a constant electric field (m^2/N), v_s is the Poisson`s ratio of the substrate, and $Y_s$ is the Young`s modulus of the substrate (N/m^2).

Since for PMN–PT material $d_{31} < 0$, $s_{13} < 0$ and d_{31} is relatively large, the effective coefficient measured for the films is lower than that of the unclamped material ($d_{33}^{eff} < d_{33}$). Generally, the characteristics of thick-film bending actuators mainly depend on the transverse piezoelectric coefficient d_{31}^{eff}. The material parameters reported in the open literature for PMN–PT thick films processed on Al_2O_3 substrates are collected in Table 1. As is evident from these data, the elastic compliance of the 0.65PMN–0.35PT thick films was higher than those of the bulk ceramics, while the piezoelectric coefficients d_{31} and d_{33} were smaller in comparison with the bulk coefficients.

As the magnitude of the electric field strength increases in 0.65PMN–0.35PT thick films the contribution of the second-order electrostrictive effect also prevails (Uršič et al., 2008a, 2008b). The equation for the strain in the 0.65PMN–0.35PT material under an applied electric field is:

$$S_i = d_{ij}E_k + M_{ij}E_k^2, \tag{5}$$

where S is the strain, E (V/m) is the electric field, d (m/V) is the piezoelectric coefficient and M (m^2/V^2) is the electrostrictive coefficient of the 0.65PMN–0.35PT material.

Coefficient (unit)	0.65PMN–0.35PT on Al_2O_3 (Uršič et al., 2008a)	0.655PMN–0.345 PT bulk ceramics (Alguero et al., 2005)
s_{11}^E (10^{-12} m²/N)	23.1	13.5
s_{33}^E (10^{-12} m²/N)	24.8	14.5
s_{12}^E (10^{-12} m²/N)	-8.20	-4.8
s_{13}^E (10^{-12} m²/N)	-10.1	-5.9
s_{44}^E (10^{-12} m²/N)	53	31.0
s_{66}^E (10^{-12} m²/N)	62.5	36.6
d_{31} (10^{-12} C /N)	-100	-223
d_{33} (10^{-12} C /N)	140–190* (Gentil et al., 2004; Kuščer et al. 2009; Kosec et al., 2007, 2010; Uršič et al., 2011b)	480

*authors present the coefficient d_{33}, of the 0.65PMN–0.35PT thick film; however, following the reported experiments this coefficient is d_{33}^{eff}

Table 1. The elastic and piezoelectric properties of the 0.65PMN–0.35PT thick films on Al_2O_3 substrates. For comparison the properties of bulk 0.655PMN–0.345PT are added.

The second-order electrostrictive effect was measured for the 0.65PMN–0.35PT thick film on the alumina substrate. Measurements of displacement vs. time at different voltage amplitudes and displacement vs. voltage amplitude for the 0.65PMN–0.35PT thick film on the Al_2O_3 substrate are shown in figs. 8 (a) and (b), respectively. The second-order electrostrictive coefficient M_{33} for the thick films is $7.6 \cdot 10^{-16}$ m²/V² (Uršič et al., 2008b). In comparison with the M_{33} of 0.65PMN–0.35PT single crystals, i. e., from 13 to $40 \cdot 10^{-16}$ m²/V² (Bookov & Ye, 2002), the measured electrostrictive coefficient for the 0.65PMN–0.35PT thick film is lower. There are several parameters that could reduce the electrostrictive coefficients of films, i.e., clamping of the film to the substrate and a lower dielectric constant in the films compared to single crystals. However, in comparison to the M_{33} value for PMN (x=0) thin films, which is $8.9 \cdot 10^{-17}$ m²/V² (Kighelman et al., 2001), the value for thick films with the MBP composition is much higher.

3.4 PMN–PT thick-film functional structures for certain applications

The designers of 0.65PMN–0.35PT thick-film functional structures for certain applications should be aware of all the above-mentioned technological effects influencing the resulting properties of thick films. Since the effective material properties of the 0.65PMN–0.35PT thick film depend not only on the material composition, but also on its compatibility with the substrate and the electrodes, and the technological parameters relating to the film processing, the characterisation of these films is required before the design phase. Due to its large responses to an applied electric field the PMN–PT material has been investigated as a promising material for actuator applications (Uršič et al., 2008a, 2008b). The disadvantage of the PMN–PT material is that it can be depoled by the application of negative electric field, due to a switch of the domain walls.

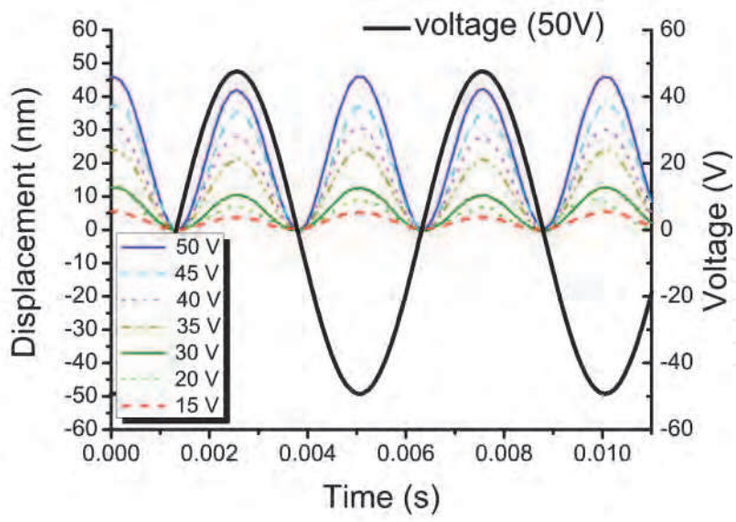

(a)

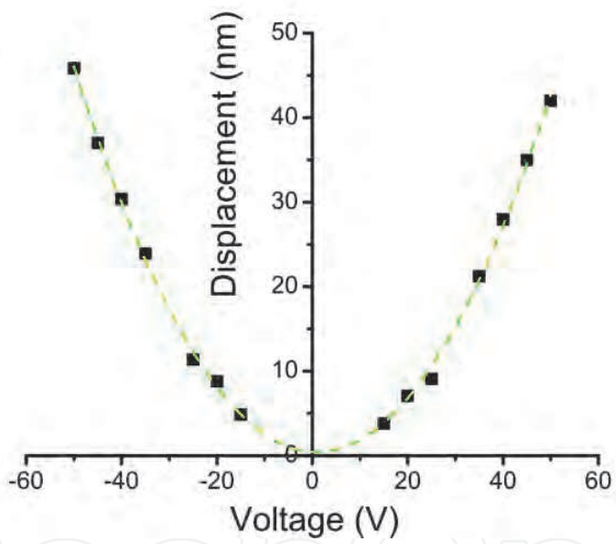

(b)

Fig. 8. (a) Measurements of displacement vs. time at different voltage amplitudes for the 0.65PMN–0.35PT thick film on the Al_2O_3 substrate. Measurement frequency 200 Hz. (b) The displacement vs. voltage amplitude for the 0.65PMN–0.35PT thick film on the Al_2O_3 substrate. The dotted line (quadratic fit) between the measured values is just a guide to the eye. (Reprinted with permission from Uršič, H. et al., J. Appl. Phys. Vol. 103, No. 12.]. Copyright [2008], American Institute of Physics).

Recently, single-crystal thick films bonded to Si substrates were prepared for high-frequency ultrasonic transducers. The transducer exhibited a good energy-conversion performance with a very low insertion loss. This insertion loss is significantly better than what could be obtained using devices with conventional piezoelectric materials, such as PZT and polyvinylidene fluoride PVDF (Peng et al., 2010).

Driven by the versatility of conventional thick-film technology, various designs of thick-film piezoelectric actuators are possible. The simplest thick-film piezoelectric actuator design is a free-standing cantilever beam that can be realized as a bimorph or multimorph multilayer structure. In combination with the materials and technologies enabling 3D structuring, even arbitrarily shaped thick-film actuator structures can be feasible. According to the type of displacement, the most common thick-film piezoelectric actuators are categorised as cantilever- (or bending) and membrane-type actuators. The bending-type actuators are generally capable of larger displacements, but exert a weak generative force. Due to the clamping to the substrate they have smaller displacements in comparison to the substrate-free structures. Furthermore, the properties of the thick films differ from those of the respective bulk ceramics; in particular, the piezoelectric properties are weaker and can even be reduced by an interaction with the reactive substrates. All these effects should be considered in the design of the structure and the technological procedure (Uršič et al., 2011c).

A novel approach to manufacturing large-displacement PMN–PT/Pt actuators by using thick-film technology based on the screen printing of the functional layers was developed (Uršič et al., 2008a). The actuators were prepared by screen-printing the PMN–PT films over the Pt electrodes directly onto Al_2O_3 substrates, which results in a poor adhesion between the electrodes and the substrates, enabling the PMN–PT/Pt thick-film composite structures to be simply separated from the substrates. In this way, "substrate-free" actuator structures were manufactured. The scheme of the cross-section and the photograph of the top view of the PMN–PT/Pt actuators are shown in fig. 9 (a) and (b). The PMN–PT/Pt actuator during a measurement of the displacement is shown in fig. 9 (c).

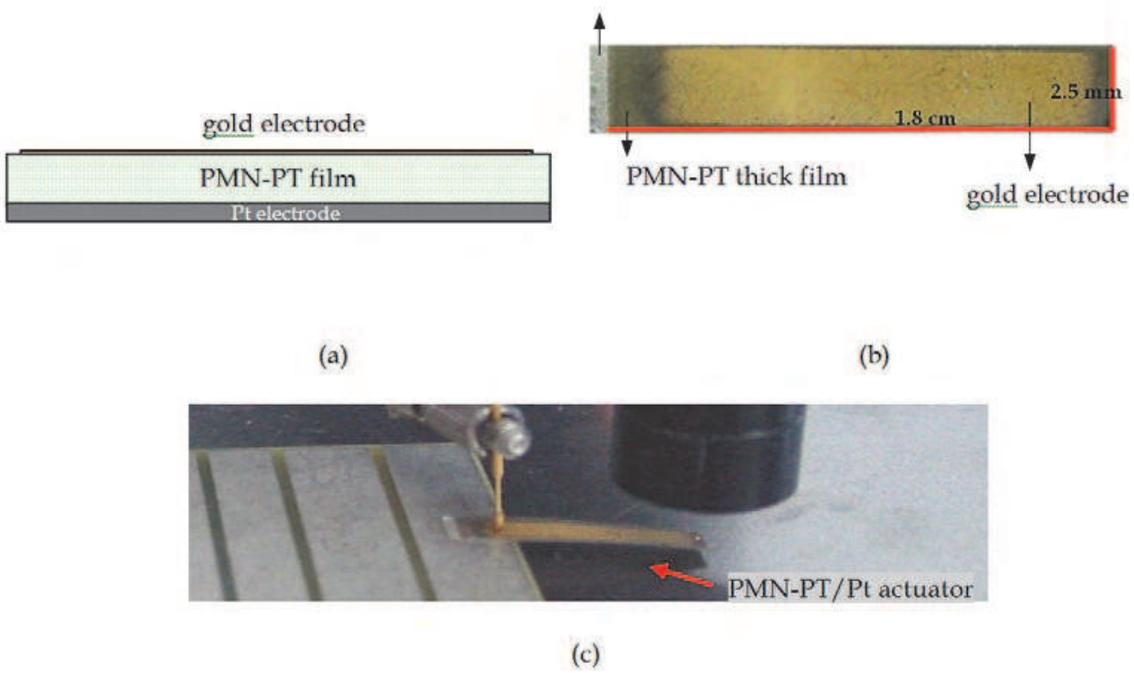

Fig. 9. (a) The scheme of the cross-section and (b) the photograph of the top view of the PMN–PT/Pt bimorph actuators. (c) The actuator during the measurement of displacement. The measurements were performed at the tip of the actuator's cantilever.

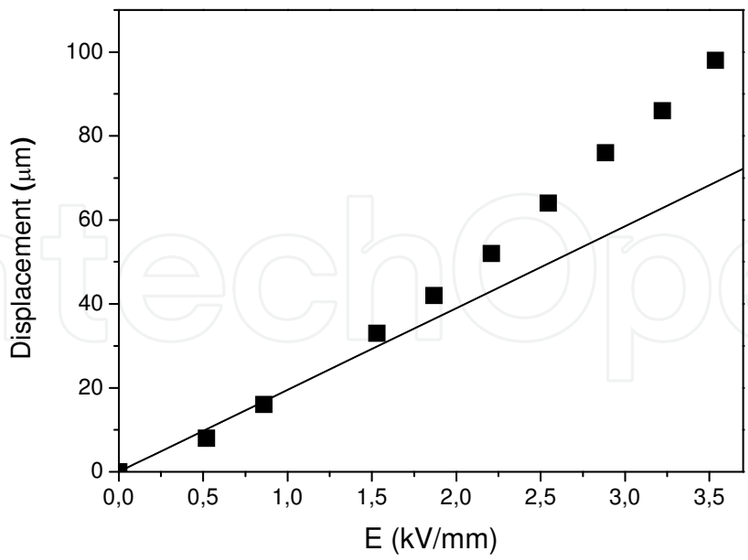

(a)

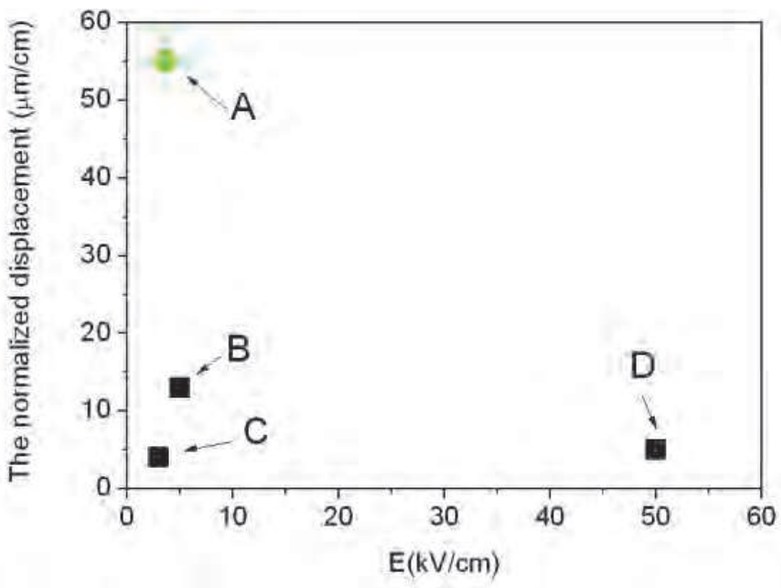

(b)

Fig. 10. (a) The bending displacement vs. applied electric field for the PMN–PT/Pt actuator and the linear finite-element model of the actuator bending (line). (b) The normalized displacement for the PMN–PT/Pt thick-film actuator in comparison with the data from the literature. Legend A: 0.65PMN–0.35PT/Pt thick-film actuator (Uršič 2008a), B: 0.65PMN–0.35PT+0.90PMN-0.10 actuator (Hall et al., 2006), C: 0.65PMN–0.35PT+0.90PMN–0.10PT actuator (Hall et al., 2005), D: PZT-thick film on alumina substrate, (Belavič et al. 2006; Zarnik et al., 2007). (Reprinted from Sens. Actuat. B Chem., 133 /2, Uršič, H. et al., A large-displacement $65Pb(Mg_{1/3}Nb_{2/3})O_3–35PbTiO_3$/Pt bimorph actuator prepared by screen printing, pp. (699–704), Copyright (2008), with permission from Elsevier).

The measurements of bending displacements were performed at the tip of the actuator's cantilever. The displacement vs. applied electric field for the PMN–PT/Pt actuator is shown in fig. 10 (a). In addition, the linear FE model of the actuator displacement is added. The measured normalized displacement (displacement per unit length) of these actuators is very high, i.e., 55 μm/cm at 3.6 kV/cm (Uršič et al., 2008a). The comparison between the normalized displacements of PMN–PT/Pt thick-film actuators and PMN–PT actuators from the literature is shown in fig. 10 (b).

The characteristics of the actuators made by using PMN–PT differ from those of the linear piezoelectric actuators (e.g., PZT actuators), mainly because of the high electrostrictive effect in the PMN–PT material. This effect takes place particularly at larger electric fields (fig. 10(a)). However, under low applied electric fields, i.e., lower than 1.5 kV/cm for the MPB compositions (Feng et al., 2004; Uršič et al., 2008a), the major effect is the linear piezoelectric effect (fig. 10(a)). Hence, at low electric fields, not just PZT, but also PMN–PT actuators show a linear response to the applied electric field. For some applications, the 1.5 kV/cm is a large input value, for example, in mobile devices where a voltage of only 10 V is normally used (Ko et al., 2006). In any case, the PMN–PT material can be appropriate for bending actuators in applications operating at higher voltages, where the linearity of the response to the applied electric field is not required.

PMN–PT thick films have many potential applications. Depending on the application, different constructions and realisations of the PMN–PT thick-film structures are possible. The state of the art in the processing of PMN–PT structures is the development of new, effective functional structures with the desired output for specific applications. There are still a number of challenges to be faced in the production of PMN–PT structures and many possibilities for further improvements in their performance to meet the industrial demands for production.

4. Conclusion

The progress in PMN–PT thick films is a consequence of the growing opportunities offered by micro-electromechanical systems. The relaxor-ferroelectric PMN–PT compositions are considered as appropriate materials for thick-film technologies, where they exhibit very good functional properties.

To form good-quality and high-performance PMN–PT thick films, a fine particle size of the PMN–PT powder is required. One way to prepare such a powder is mechanochemical synthesis. The most commonly used method for the deposition of PMN–PT-based thick films is screen-printing; however, a few experiments with electrophoretic deposition, the hydrothermal process and sol-gel were also reported. The proper selection of the materials, including the compatibility of the functional PMN–PT material with the electrodes and the substrates, is among the most important factors for the successful processing of PMN–PT thick-film structures.

The process-induced residual stresses in the thick-film structure and the possible reactions between the thick film and the reactive substrate may change considerably the functional properties of the films. The clamping of the PMN–PT film to the substrate influences the electro-active response of the film. In addition, the interactions between the PMN–PT film and the substrate may result in a deterioration of the material's functional properties.

New research has shown that the thermal residual stresses in the films have a great influence on the structural and electrical properties of the films. The difficulty is in separating the influence of the thermal stresses from the influence of the microstructure, while the thermal stresses and the microstructure have a great influence on the properties of the films. However, lately the phase composition of 0.65PMN–0.35PT thick films was compared to the phase composition of 0.65PMN–0.35PT bulk ceramics with a similar microstructure. In this way it was shown that the thermal residual stresses have a great influence on the phase composition of the thick films and, furthermore, that in PMN–PT thick films the morphotropic phase boundary shifts under the compressive stress.

PMN–PT thick films have many potential applications, although their production faces many challenges arising from the successful integration of different material systems. From all the latest discoveries we can conclude that a proper selection of a material compatible with the functional PMN–PT layer is of key importance for the successful processing of PMN–PT thick films and their integration into applicable structures. With the proper selection of the substrate material, the designer of PMN–PT thick-film structures can control the structural and electrical properties of the active thick film. Structures including piezo-active PMN–PT single-crystal layers and large displacement "substrate free" PMN–PT/Pt thick-film actuators were reported.

The state of the art is the development of new, effective methods for processing PMN–PT thick films with even better functional properties, new procedures for the characterization of thick films and the investigation of innovative design solutions for PMN–PT thick-film structures in different applications. There are still a number of challenges to be faced in the production of PMN–PT thick-film structures and the many possibilities for further improvements in their performance to meet the industrial demands for mass production. However, the basis for future investigations in this field would seem to be the development of new relaxor-ferroelectric thick films with the desired properties for specific applications.

5. Acknowledgment

The financial support of the Slovenian Research Agency in the frame of the program Electronic Ceramics, Nano-, 2D and 3D Structures (P2-0105) is gratefully acknowledged.

6. References

Alguero, M.; Alemany, C.; Pardo, L.; Thi, M. P. (2005). Piezoelectric Resonances, Linear Coefficients and Losses of Morphotropic Phase Boundary Pb(Mg1/3Nb2/3)O3–PbTiO3 Ceramics, *J. Am. Ceram. Soc.*, Vol. 88, No. 10, (May 2005), pp. (2780–2787), doi: 10.1111/j.1551-2916.2005.00514.x

Alguero, M.; Moure, A.; Pardo, L.; Holc, J. & Kosec M., (2006). Processing by mechanosynthesis and properties of piezoelectric $Pb(Mg_{1/3}Nb_{2/3})O_3$–$PbTiO_3$ with different compositions, *Acta Materialia*, Vol. 54, No. 2, (September 2005), pp. (501–511), doi: 10.1016/j.actamat.2005.09.020

Alguero, M.; Ricote, J. & Jimenez, R., (2007). Size effect in morphotropic phase boundary $Pb(Mg_{1/3}Nb_{2/3})O_3$– $PbTiO_3$, *Appl. Phys. Lett.*, Vol. 91, No. 12, (August 2007), pp. (112905 1–3), doi: 10.1063/1.2778471

Akiyama,Y.; Yamanaka, K.; Fujisawa, E. & Kowata, Y. (1999). Development of lead zirconate titanate family thick films on various substrates, *Jpn. J.Appl. Phys.*, Vol. 38, No. 9B, (June 1999), pp. (5524–5527), doi: 10.1143/JJAP.38.5524

Belavič, D.; Zarnik, M.S.; Holc, J.; Hrovat, M.; Kosec, M.; Drnovšek, S.; Cilenšek, J. & Maček S. (2006). Properties of lead zirconate titanate thick-film piezoelectric actuators on ceramic substrates, *Int. J. Appl. Ceram. Technol.*, Vol. 3, No. 6, (November 2006), pp. (448-454), doi: 10.1111/j.1744-7402.2006.02105.x

Bokov, A. A. & Ye, Z. G. (2002). Giant electrostriction and stretched exponential electromechanical relaxation in 0.65Pb(Mg1/3Nb2/3)O3–0.35PbTiO3 crystals, *J. Appl. Phys.*, Vol. 91, No. 10, (February 2002), pp. (6656-6661), doi: 10.1063/1.1471371

Carreaud, J.; Gemeiner, P.; Kiat, J. M.; Dkhil, B.; Bogicevic, C.; Rojac, T. & Malič, B. (2005). Size-driven relaxation and polar states in $PbMg_{1/3}Nb_{2/3}O_3$-based system, *Phys. Rev. B*, Vol. 72, No. 17, (November 2005), pp. (174115 1–6), doi: 10.1103/PhysRevB.72.174115

Chen, X.; Fan, H.; Liu, L. & Ke, S. (2008). Low-temperature growth of lead magnesium niobate thick films by a hydrothermal process, *Ceramics International*, Vol. 34, No. 4, (October 2007) pp. (1063–1066), doi: 10.1016/j.ceramint.2007.09.080

Chen, J.; Fan, H. Q.; Chen, X. L.; Fang, P.; Yang C. & Qiu, S. (2009a). Fabrication of pyrochlore-free PMN-PT thick films by electrophoretic deposition, *Journal of Alloys and Compounds*, Vol. 471, No. 1-2, (June 2008), pp. (L51-L53), doi: 10.1016/j.jallcom.2008.06.088

Chen, J.; Fan, H.; Ke, S.; Chen, X.; Yang C. & Fang P. (2009b). Relaxor behavior and dielectric properties of lead magnesium niobate–lead titanate thick films prepared by electrophoresis deposition, *Journal of Alloys and Compounds*, Vol. 478, No. 1-2, (December 2008) pp. (853–857), doi: 10.1016/j.jallcom.2008.12.041

Cross, L. E. (1987). Relaxor ferroelectrics, *Ferroelectrics,* Vol. 76, No. 3, (June 1987), pp. (241–67).

Damjanovic, D. (2008). Lead-based piezoelectric materials, In: *Piezoelectric and Acoustic Materials for Transducer Applications*, Springer, Editors: A. Safari, E. K. Akdogan, Springer Science+Business Media, ISBN 978-0-387-76538-9, LLC 2008.

Davis, M.; Damjanovic, D. & Setter, N. (2006). Electric-field-, temperature-, and stress-induced phase transitions in relaxor ferroelectric single crystals, *Phys. Rev. B* Vol. 73, No. 1, (October 2005), pp. (014115 1–16), doi: 10.1103/PhysRevB.73.014115

Fan, H.; Chen, J. & Chen, X. (2008). Preparation and characterization of relaxor-based ferroelectric thick films with single perovskite phase, *Key Engineering Materials*, Vol. 368, (February 2008) pp. (24-26), doi: 10.4028/www.scientific.net/KEM.368-372.24

Feng, Z.; He, Z.; Xu, H.; Luo, H. & Yin, Z. (2004). High electric-field-induced strain of Pb(Mg1/3Nb2/3)O3–PbTiO3 crystals in multilayer actuators, *Solid State Communications,* Vol. 130, No. 8, (September 2003) pp. (557-562), doi: 10.1016/j.ssc.2004.03.006

Gentil, S.; Damjanovic, D. & Setter, N. (2004). $Pb(Mg_{1/3}Nb_{2/3})O_3$ and (1-x)$Pb(Mg_{1/3}Nb_{2/3})O_3$-x$PbTiO_3$ relaxor ferroelectric thick films: processing and electrical characterization,

J. Electroceramics, Vol. 12, No. 3, (July, 2003), pp. (151–161), doi: 10.1023/B:JECR.0000037720.39443.e3

Gentil, S.; Damjanovic, D. & Setter N. (2005). Development of relaxor ferroelectric materials for screen-printing on alumina and silicon substrates, *J. Eur. Ceram. Soc.*, Vol. 25, No. 12, (April 2005), pp. (2125–2128), doi: 10.1016/j.jeurceramsoc.2005.03.210

Hall, A.; Allahverdi, M.; Akdogan, E. K. & Safari, A. (2005). Piezoelectric/electrostrictive multimaterial PMN-PT monomorph actuators, *J. Eur. Ceram. Soc.*, Vol. 25, No. 12, (April 2005), pp. (2991-2997), doi: 10.1016/j.jeurceramsoc.2005.03.196

Hall, A.; Allahverdi, M.; Akdogan, E. K. & Safari, A. (2006). Fatigue properties of piezoelectric-electrostrictive $Pb(Mg_{1/3},Nb_{2/3})O_3$-$PbTiO_3$ monolithic bilayer composites, *J. Appl. Phys.*, Vol. 100, No. 9, (July 2006), pp. (094105 1-7), doi: 10.1063/1.2358329

Holc, J.; Hrovat, M & Kosec, M. (1999). Interactions between alumina and PLZT thick films, *Mat. Res. Bull.*, Vol. 34, No. 14-15, (March 1999), pp. (2271-2278), doi: 10.1016/S0025-5408(99)00227-5

Lefki, K. & Dormans, G. J. M (1994). Measurement of piezoelectric coefficients in ferroelectric thin films, *J. Appl. Phys.* Vol. 76, No. 3, (April 1994), pp. (1764–1767), doi: 10.1063/1.357693

Leite, E. R.; Scotch, A. M.; Khan,A.; Chan, H. & Harmer, M. P. (2002). Chemical heterogeneity in PMN–35PT ceramics and effects on dielectric and piezoelectric properties, *J. Am. Ceram. Soc.*, Vol. 85, No. 12, (December 2002), pp. (3018-24), doi: 10.1111/j.1151-2916.2002.tb00572.x

Kelly, J.; Leonard, M.; Tantigate, C. & Safari, A. (1997). Effect of composition on the electromechanical properties of $(1-x)Pb(Mg_{1/3}\ Nb_{2/3})O_3$– $xPbTiO_3$ ceramics, *J. Am. Ceram. Soc.*, Vol. 80, No. 4, (April 1997), pp. (957-964), doi: 10.1111/j.1151-2916.1997.tb02927.x

Kighelman, Z.; Damjanovic, D. & Setter, N. (2001). Electromechanical properties and self-polarization in relaxor Pb(Mg1/3Nb2/3)O3 thin films, *J. Appl. Phys.*, Vol. 89, No. 2, (October 2001), pp. (1393-1401), doi: 10.1063/1.1331339

Ko, B.; Jung, J.S.; Lee & S. Y. (2006). Design of a slim-type optical pick-up actuator using PMN-PT bimorphs, *Smart Mater. Struct.*, Vol. 15, No. 6, (September 2006), pp. (1912-1918), doi: 10.1088/0964-1726/15/6/047

Kosec, M.; Holc, J.; Malič, B. & Bobnar, V. (1999). Processing of high performance lead lanthanum zirconate titanate thick films, *J. Eur. Ceram. Soc.*, Vol. 19, No. 6/7, (June 1999), pp. (949-954), doi: 10.1016/S0955-2219(98)00351-3

Kosec, M.; Holc, J.; Kuščer, D. & Drnovšek, S. (2007). $Pb(Mg_{1/3}Nb_{2/3})O_3$– $PbTiO_3$ thick films from mechanochemically synthesized powder, *J. Eur. Ceram. Soc.*, Vol. 27, No. 13-15, (March 2007), pp. (3775-2778), doi: 10.1016/j.jeurceramsoc.2007.02.025

Kosec, M.; Uršič, H.; Holc, J.; Kuščer, D. & Malič, B. (2010). High-performance PMN–PT thick films, *IEEE Trans. Ultrason. Ferroelectr. Freq. Control*, Vol. 57, No. 10, (October 2010), pp. (2205-2212), doi: 10.1109/TUFFC.2010.1679

Kuščer, D. & Kosec, M. (2009) 0.65Pb(Mg1/3Nb2/3)O3–0.35PbTiO3 thick films prepared by electrophoretic deposition from an ethanol-based suspension, *J. Eur. Ceram. Soc.*, Vol. 30, No. 6, (April 2010), pp. (1437–1444), doi: 10.1016/j.jeurceramsoc.2009.11.002

Kuščer, D; Skalar, M; Holc, J; Kosec, M. (2008). Processing and properties of 0.65Pb(Mg1/3Nb2/3)O3–0.35PbTiO3 thick films, *J. Eur. Ceram. Soc.*, Vol. 29, No. 1, (June, 2008), pp. 105-113, doi: 10.1016/j.jeurceramsoc.2008.06.010

Noheda, B.; Cox, D. E.; Shirane, G.; Park, S. E.; Cross, L. E. & Zhong, Z. (2001). Polarization rotation via a monoclinic phase in the piezoelectric 92% $PbZn_{1/3}Nb_{2/3}O_3$-8% $PbTiO_3$, *Phys. Rev. Lett.*, Vol. 86, No. 17, (April 2001), pp. (3891-3894), doi: 10.1103/PhysRevLett.86.3891

Ohring, M. (1992). *The material science of thin films* (1992), Academic Press, ISBN 0-12-524990, New York.

Park, S. E. & Shrout, T. R., (1997a). Ultrahigh strain and piezoelectric behavior in relaxor based ferroelectric single crystals, *J. Appl. Phys.*, Vol. 82, No. 4 (May 1997) pp. (1804–1811),doi: 10.1063/1.365983

Park, S. E. & Shrout, T. R. (1997b). Relaxor based ferroelectric single crystals for electro-mechanical actuators, *Mat. Res. Innovat.*, Vol. 1, No. 1 (March 1997), pp. (20–25), doi: 10.1007/s100190050014

Peng, J.; Lau, S. T.; Chao, C.; Dai, J. Y.; Chan, H. L. W.; Luo, H. S.; Zhu, B. P.; Zhou, Q. F. & Shung, K. K. (2010) PMN-PT single crystal thick films on silicon substrate for high-frequency micromachined ultrasonic transducers, *Appl. Phys. A*, Vol. 98, No. 1, (August 2010), pp. (233–237), doi: 10.1007/s00339-009-5381-1

Singh, A. K. & Pandey, D. (2003). Evidence for M_B and M_C phases in the morphotropic phase boundary region of (1-x)[$Pb.Mg_{1/3}Nb_{2/3}O_3$]-x$PbTiO_3$: A Rietveld study, *Phys. Rev. B*, Vol. 67, No. 6, (November 2002), pp. (064102 1–12), doi: 10.1103/PhysRevB.67.064102

Shrout, T. R.; Chang, Z. P.; Kim, N. & Markgraf, S. (1990) Dielectric behavior of single crystals near the (1-X) Pb(Mg1/3Nb2/3)O3-(x) PbTiO3 morphotropic phase boundary, *Ferroelectrics Letters*, Vol. 12, No. 3, (September 1990), pp. (63-69), doi: 10.1080/07315179008201118

Swartz, S. L. & Shrout, T. R. (1982). Fabrication of perovskite lead magnesium niobate. *Mat. Res. Bull.*, Vol. 17, No. 10, (October 1982), pp. (1245–1250), doi: 10.1016/0025-5408(82)90159-3

Swartz, S. L.; Shrout, T. R.; Schulze, W. A. & Cross, L. E. (1984). Dielectric properties of lead-magnesium niobate ceramics. *J. Am. Ceram. Soc.*, Vol. 67, No. 5, (May 1984), pp. (311–315), doi: 10.1111/j.1151-2916.1984.tb19528.x

Uchino, K; Nomura, S.; Cross, L. E.; Jang, S. E. & Newnham, R. E. (1890). Electrostrictive effect in lead magnesium niobate single crystals, *J. Appl. Phys.*, Vol. 51, No. 2, (February 1980), pp. 1142-1146, doi: 10.1063/1.327724

Uršič, H.; Hrovat, M.; Holc, J.; Zarnik, M. S.; Drnovšek, S.; Maček, S. & Kosec, M. (2008a). A large-displacement 65Pb($Mg_{1/3}Nb_{2/3}$)O_3–35$PbTiO_3$/Pt bimorph actuator prepared by screen printing, *Sens. Actuat. B Chem.*, Vol. 133, No. 2, (March 2008), pp. (699–704), doi: 10.1016/j.snb.2008.04.004

Uršič, H.; Škarabot, M.; Hrovat, M.; Holc, J.; Skalar, M.; Bobnar, V.; Kosec, M. & Muševič, I. (2008b). The electrostrictive effect in ferroelectric 0.65Pb($Mg_{1/3}Nb_{2/3}$–0.35$PbTiO_3$ thick films, *J. Appl. Phys.*, Vol. 103, No. 12, (April 2008), pp. (124101 1–4), doi: 10.1063/1.2938848

Uršič, H; Lowe, M.; Stewart, M.; Hrovat, M.; Belavič, D.; Holc, J.; Zarnik, M. S.; Kosec, M. & Cain, M. (2008c), PZT thick films on different ceramic substrates; piezoelectric measurements, *J. Electroceram.,* Vol. 20, No. 1, (September 2007), pp. (11–16), doi: 10.1007/s10832-007-9327-8

Uršič, H.; Hrovat, M.; Holc, J.; Tellier., J.; Drnovšek, S.; Guiblin, N.; Dkhil; B. & Kosec, M. (2010). Influence of the substrate on the phase composition and electrical properties of 0.65PMN–0.35PT thick films, *J. Eur. Ceram. Soc.,* Vol. 30, No. 10, (April 2010), pp. (2081–2092), doi: 10.1016/j.jeurceramsoc.2010.04.010

Uršič, H.; Tellier, J.; Hrovat, M.; Holc, J.; Drnovšek, S.; Bobnar, V.; Alguero, M; & Kosec, M. (2011a). The effect of poling on the properties of 0.65Pb(Mg1/3Nb2/3)O3–0.35PbTiO3 ceramics, *Jpn. J. Appl. Phys.*, Vol. 50, No. 3, (December 2010), pp. (035801 1-6), doi: 10.1143/JJAP.50.0358011

Uršič, H; Zarnik, M. S.; Tellier, J.; Hrovat, M.; Holc, J. & Kosec, M. (2011b). The influence of thermal stresses on the phase composition of $0.65Pb(Mg_{1/3}Nb_{2/3})O_3–0.35PbTiO_3$ thick films, *J. Appl. Phys.* Vol. 109, No. 1, (November 2010), pp. (014101 1-5), doi: 10.1063/1.3526971

Uršič, H; Zarnik, M. S. & Kosec, M. (2011c). $Pb(Mg_{1/3}Nb_{2/3})O_3–PbTiO_3$ (PMN–PT) material for actuator applications, *Smart Materials Research*, in press, accepted January 2011, Article ID 452901, doi:10.1155/2011/452901

Vikhnin, V. S.; Blinc, R. & Pirc, R. (2003). Mechanisms of electrostriction and giant piezoelectric effect in relaxor ferroelectrics, *J. Appl. Phys.*, Vol. 93, No. 12, (March 2003), pp. (9947-9952), doi: 10.1063/1.1575915

Wu, A.; Vilarinho, P. M. & Kholkin, A. (2007) Low temperature preparation of ferroelectric relaxor composite thick films, *J. Am. Ceram. Soc.*, Vol. 90, No. 4, (March 2007), pp. (1029–1037), doi: 10.1111/j.1551-2916.2007.01587.x

Xia, Z.; Wang, L.; Yan, W.; Li, Q. & Zhang, Y. (2007) Comparative investigation of structure and dielectric properties of $Pb(Mg_{1/3}Nb_{2/3})O_3–PbTiO_3$ (65/35) and 10% $PbZrO_3$-doped $Pb(Mg_{1/3}Nb_{2/3})O_3–PbTiO_3$ (65/35) ceramics prepared by a modified precursor method, *Mat. Res. Bull.,* Vol. 42, No. 9, (September 2007), pp. (1715-1722), doi: 10.1016/j.materresbull.2006.11.024

Zarnik M. S.; Belavič, D. & S. Maček. (2007). Evolution of the constitutive material parameters for the numerical modeling of structures with lead-zirconate-titanate thick films, *Sens. Actuat. A*, Vol. 136, No. 2, (January 2007), pp. (618-628), doi: 10.1016/j.sna.2007.01.010

Zarnik, M. S.; Belavič, D.; Uršič, H. & Maček S. (2008). Numerical modelling of ceramic mems structures with piezoceramic thick films, *J. Electroceram.*, Vol. 20, No. 1, (September 2007), pp. (3–9), doi: 10.1007/s10832-007-9329-6

Zhang, R.; Jiang, B. & Cao, W. (2001). Elastic, piezoelectric, and dielectric properties of multidomain 0.67Pb(Mg1/3Nb2/3)O3–PbTiO3 single crystals, *J. Appl. Phys.,* Vol. 90, No.7, (June 2001), pp. (3471-3475), doi: 10.1063/1.1390494

Zhao, J.; Zhang, Q. M.; Kim, N. & Shrout, T. (1995). Electromechanical properties of relaxor ferroelectric lead magnesium niobate-lead titanate ceramics, *Jpn. J. Appl. Phys.* Vol. 34, No. 10, (July 1995), pp. (5658-5663), doi: 10.1143/JJAP.34.5658

Zhu, B.; Han, J.; Shi, J.; Shung, K. K.; Wei, Q.; Huang, Y.; Kosec, M. & Zhou, Q. (2010) Lift-Off PMN–PT Thick Film for High-Frequency Ultrasonic Biomicroscopy, *J. Am. Ceram. Soc.,* Vol. 93, No. 10, (August 2010), pp. (2929–2931), doi: 10.1111/j.1551-2916.2010.03873.x

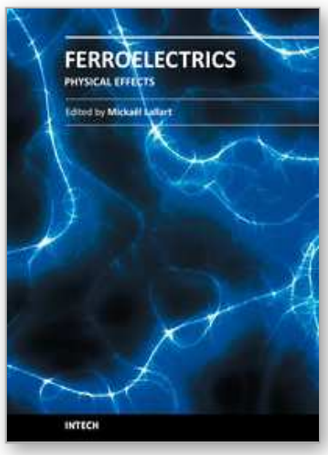

Ferroelectrics - Physical Effects

Edited by Dr. MickaÃ«l Lallart

ISBN 978-953-307-453-5
Hard cover, 654 pages
Publisher InTech
Published online 23, August, 2011
Published in print edition August, 2011

Ferroelectric materials have been and still are widely used in many applications, that have moved from sonar towards breakthrough technologies such as memories or optical devices. This book is a part of a four volume collection (covering material aspects, physical effects, characterization and modeling, and applications) and focuses on the underlying mechanisms of ferroelectric materials, including general ferroelectric effect, piezoelectricity, optical properties, and multiferroic and magnetoelectric devices. The aim of this book is to provide an up-to-date review of recent scientific findings and recent advances in the field of ferroelectric systems, allowing a deep understanding of the physical aspect of ferroelectricity.

INTECH
open science | open minds

InTech Europe
University Campus STeP Ri
Slavka Krautzeka 83/A
51000 Rijeka, Croatia
Phone: +385 (51) 770 447
Fax: +385 (51) 686 166
www.intechopen.com

InTech China
Unit 405, Office Block, Hotel Equatorial Shanghai
No.65, Yan An Road (West), Shanghai, 200040, China
中国上海市延安西路65号上海国际贵都大饭店办公楼405单元
Phone: +86-21-62489820
Fax: +86-21-62489821

IntechOpen